CORROSION IN LITHIUM-STAINLESS STEEL THERMAL-CONVECTION SYSTEMS*

P. F. Tortorelli, J. H. DeVan, J. E. Selle

Metals and Ceramics Division
Oak Ridge National Laboratory
Oak Ridge, Tennessee 37830

CONF-800401--1

ABSTRACT

The corrosion of types 304L and 316 austenitic stainless steel by flowing lithium has been studied in thermal-convection loops operated at 500-650°C. Both weight and compositional changes were measured on specimens distributed throughout each loop and were combined with metallographic examinations to evaluate the corrosion processes. The corrosion rate and mass transfer characteristics did not significantly differ between the two austenitic stainless steels. Addition of 500 or 1700 wt ppm N to purified lithium did not increase the dissolution rate or change the attack mode of type 316 stainless steel. Adding 5 wt % Al to the lithium reduced the weight loss of this steel by a factor of 5 relative to a pure lithium thermal-convection loop.

INTRODUCTION

The corrosion of structural materials by molten alkali metals has been studied for over three decades. While most of this effort has concentrated on Na for breeder reactor applications, some work was done on Li corrosion in the 1950s and 60s in support of the aircraft nuclear propulsion program and successor space-related programs.[1,2] In recent years, a renewed interest in Li compatibility has arisen because of the possible uses of Li as a coolant and/or tritium-breeding fluid in fusion reactors. A review of the literature[2] on Li corrosion

EB

*Research sponsored by the Office of Fusion Energy, U.S. Department of Energy, under contract W-7405-eng-26 with Union Carbide Corporation.

of Fe-base alloys revealed areas needing clarification and/or further investigation in view of fusion requirements. The present program was initiated to study thermal-gradient mass transfer of stainless steels in flowing Li. This paper presents results on the effects of alloy composition, temperature, and additives to the Li on the corrosion of austenitic stainless steels by slowly-moving Li.

EXPERIMENTAL PROCEDURES

As-received Li was purified before its use in the loop experiments. The purification involved cold-trapping and subsequent heating at about 815°C for 100 h in a Ti-lined pot containing ultrahigh-purity Zr foil. This procedure reduced the nitrogen and oxygen concentrations to 30–80 wt ppm and 30–130 ppm, respectively. A typical analysis of the Li used in the loops is given in Table I.

TABLE I. TYPICAL ANALYSIS OF THE LITHIUM

Element	Content (wt %)	Element	Content (wt %)
Na	0.005	Fe	0.001
K	0.005	Al	0.001
Cl	0.005	Li	99.98
Si	0.001	N	0.003–0.010
Ca	0.001	O	0.003–0.013

The thermal-convection loops used in these experiments were in the approximate form of a 0.8-m-high by 0.4-m-wide parallelogram and were fabricated from stainless

stainless steel tubing. Figure 1 is a schematic drawing of a typical loop. Strings of interlocking 25 mm by 12 mm coupons of the same composition as the tubing were placed in both vertical legs of the loops and in some cases in the lower horizontal leg. The temperature profile around the loop was controlled to maintain naturally convective flow with a temperature difference of about 200°C across the circuit. Temperatures were continuously monitored at four points (see Fig. 1) by thermocouples in stainless steel sheaths located in the flowing Li. The Li velocity was determined by heating a small spot on the loop wall and measuring the time for the heat pulse to cause a temperature rise at a thermocouple located at a known

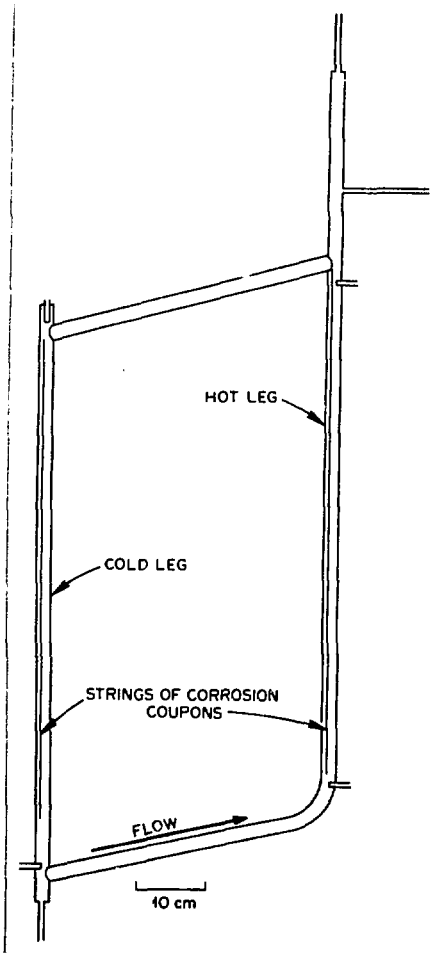

FIGURE 1. Thermal-Convection Loop.

distance downstream. The measured velocities were in reasonable agreement with velocities calculated from heat balances around the loop.[3]

The loops and insert specimens were tested as solution annealed. The weights of the insert specimens were measured before and after each loop test to yield profiles of weight change as a function of loop position. Additionally, the ferrite content of each coupon was measured after exposure to the flowing Li by determining surface magnetic susceptibility. Changes in the composition of the near-surface regions of the specimens were determined by x-ray fluorescence, while optical and scanning electron microscopy were used to characterize microstructural and topological changes caused by Li exposure. Various sections of the loop tubing were also examined metallographically. This verified that effects recorded on insert specimens were representative of those occurring at the adjoining loop wall.

Nine thermal-convection loops were operated under the conditions listed in Table II. Loops 1 and 4 were used to establish baseline corrosion data for types 304L and 316 stainless steel, respectively.

TABLE II. OPERATING CONDITIONS OF THE LITHIUM THERMAL-CONVECTION LOOPS[a]

Loop	Alloy	Additive (wt %)	Max Temp (°C)	T (°C)
1	304L	None	600	200
2	316	None	500	200
3	316	None	550	200
4	316	None	600	200
5	316	None	650	200
6[b]	316	None	600	200
7	316	0.05 N	590	170
8	316	0.17 N	600	200
9	316	5.00 Al	600	200

[a]Average Li velocity = 16 mm/s.
[b]Operated 10,000 h. All others 3,000 h.

The Li in loop 8 was inadvertently contaminated by ambient air during filling, thereby yielding data characteristic of flowing N-contaminated (1700 wt ppm) Li (with 200 ppm O). Loop 6 was a longer test (10,000 h) of type 316 stainless steel, while loops 2, 3, and 5 were also tests of type 316 but operated at different maximum temperatures. Planned additions of Al (as wire wrapped around the coupon in the hot leg) and Li_3N to the Li were made in loops 9 and 7, respectively, to study their effects on mass transport of type 316 stainless steel.

RESULTS

The weight changes of the corrosion coupons revealed transfer of material from the hotter to the cooler regions in all loops. The extent of this transfer and the relative areas of dissolution and deposition depend on several factors such as time, temperature, and additives to the Li. Figure 2 illustrates the dependence of mass transfer on the maximum loop operating temperature for type 316 stainless steel. Weight changes are plotted as a function of the distance from the bottom of the cold leg (the coldest point) in the direction of Li flow (up the heated leg). The maximum weight loss increased by a factor of 4.6 as the maximum loop temperature (T_{max}) increased from 500 to 650°C. Figure 3 compares the effects of Ni and Al additions to the Li on mass trans-fer in type 316 stainless steel loops. The Al addition inhibited corrosion, while the presence of Ni in Li affected the relative areas of dissolution and deposition but did not increase the maximum weight loss. The mass transfer characteristics of Li in types 304L and 316 stainless steel loops are compared in Fig. 4. Also shown are data from

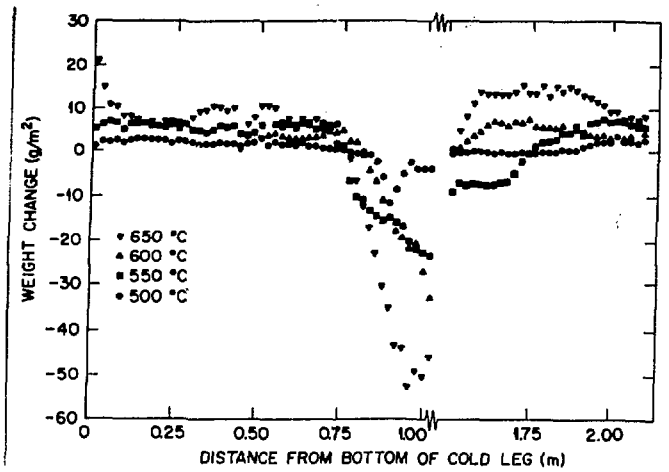

FIGURE 2. Weight Changes in 3000 h vs Loop Position for Lithium-Type 316 Stainless Steel Loop at Different Maximum Temperatures.

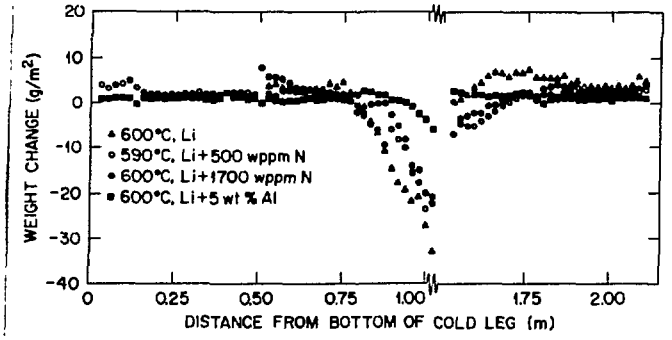

FIGURE 3. Weight Changes in 3000 h vs Loop Position for Lithium plus Additivies in Type 316 Stainless Steel Loop.

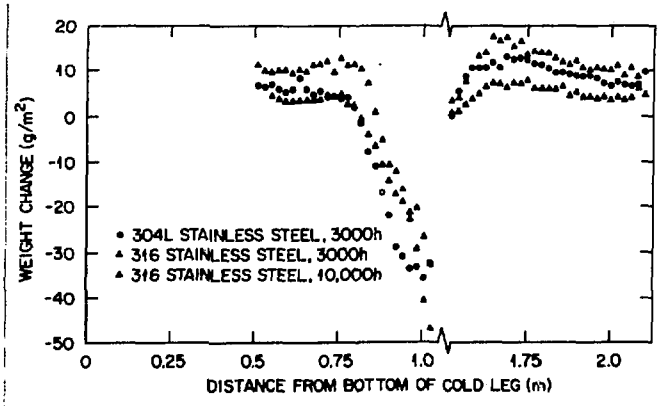

FIGURE 4. Weight Changes vs Loop Position for Lithium-Stainless Steel Loop, Comparing Alloys and Operating Times; T_{max} = 600°C.

a type 316 stainless steel loop that operated for 10,000 h. While the weight changes from the 10,000-h test are greater than the corresponding 3000-h data, the corrosion rate is considerably less.

Table III compares the maximum weight losses among the loop tests and also the loop positions at which zero weight changes were recorded (balance points). The latter points are designated X_1 and X_2 in the heated and cooled sections, respectively. A consideration of these qualities for each loop is required for a complete analysis of the results (see DISCUSSION). The balance points are defined to be the positions in the loop where the dissolution and deposition rates were equal. The locations of these points were determined from the intersections of the abscissa with the weight change vs position curves drawn through the measured points. Note that the distance from X_1 to X_2, measured in the direction of Li flow, divided by the total circuit length (2.5 m) yields the fraction of surface area over which dissolution occured.

TABLE III. MASS TRANSFER DATA FOR LITHIUM-STAINLESS STEEL THERMAL-CONVECTION LOOPS

Loop[a]	Maximum Weight Loss (g/m^2)	Balance Points, m[b]	
		Hot Leg X_1	Cold Leg X_2
1	35.6	0.81	1.55
2	11.4	0.79	1.54
3	23.4	0.76	1.76
4	32.7	0.81	1.51
5	52.4	0.76	1.52
6	47.1	0.87	1.50
7	23.4	0.80	1.69
8	20.6	0.87	1.67
9	5.9	0.95	<1.50

[a]Operating conditions in Table II.
[b]Measured from bottom of cold leg in direction of lithium flow; total circuit length is 2.5 m.

One side of each insert specimen was analyzed by x-ray fluorescence to determine the near-surface concentration of Fe, Ni, and Cr. Concentrations at equivalent positions around the nine test loops are compared in Table IV in terms of the ratio of the elemental surface concentration of the coupon at T_{max} to the surface concentration of that element in a control specimen. An example of surface concentrations as a function of loop position is shown in Fig. 5 for a type 316 stainless steel loop operated for 3000 h at a maximum temperature of 600°C. The hotter loop surfaces of all loops were depleted of Cr and Ni. The profiles of surface concentration can be used to establish the loop positions at which the content of a given element did not change from the before-test content. These are determined similarly to the weight change balance points and are listed in Table IV.

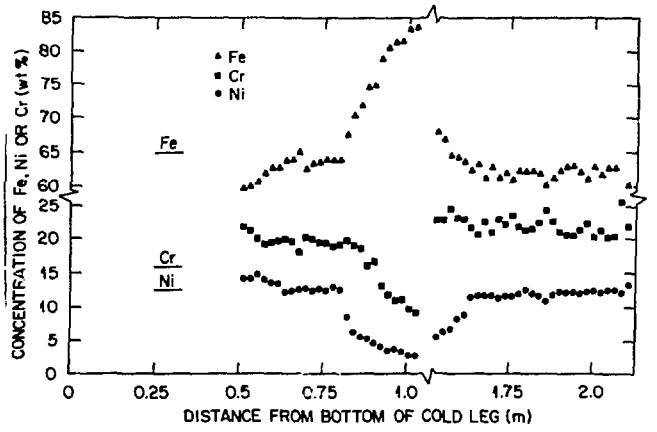

FIGURE 5. Surface Concentration vs Loop Position for Lithium-Type 316 Stainless Steel Loop Operated 3000 h with T_{max} = 600°C.

The magnetic susceptibilities of loop coupons with weight losses were measured and translated into qualitative estimates of ferrite content in the near-surface region. The amount of ferrite correlated directly

TABLE IV. X-RAY FLUORESCENCE DATA FOR LITHIUM-STAINLESS STEEL THERMAL-CONVECTION LOOPS

Loop	Concentration Ratio[a]		Balance Point Location,[b] m					
			Hot Leg			Cold Leg		
	Ni	Cr	Fe	Cr	Ni	Fe	Cr	Ni
1	0.17	0.37	0.80	0.81	0.70	1.53	1.51	1.94
2	0.24	0.91	0.78	0.98	0.79	1.75		1.77
3	0.14	0.65	0.77		0.78	1.78		1.75
4	0.19	0.58	0.81	0.90	0.72	1.57	<1.50	1.64
5	0.16	0.42	0.79	0.78	0.74	1.55	1.53	1.86
6	0.18	0.48	0.83	0.91	0.80		<1.50	1.81
7	0.25	0.55		0.85	0.79		1.52	1.81
8	0.33	0.74	0.77	0.93	0.77	1.75	1.77	1.74
9	1.0	0.86						

[a]Ratio of surface percentage on coupon at T_{max} to percentage in unexposed material.
[b]Loop locations where elemental concentration equals that of control unexposed specimens; measured from bottom of cold leg in direction of lithium flow; total circuit length is 2.5 m. Blanks indicate that the details of the fluorescence profiles did not allow an accurate determination of that balance point.

with the weight loss, as shown in Fig. 6. Ferrite was also detected on certain coupons, located immediately downstream of the heated section, that gained weight.

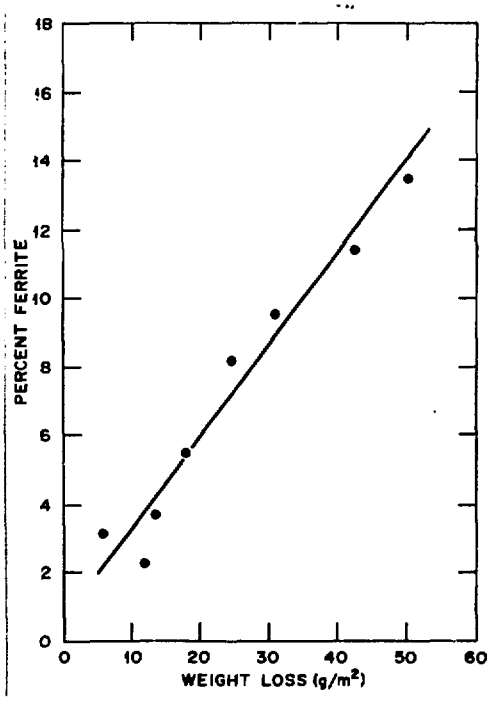

FIGURE 6. Ferrite Concentration vs Weight Loss for Lithium Type 316 Stainless Steel Loop Operated 3000 h at T_{max} = 600°C.

Cross sections of representative coupons from each of the test loops were metallographically examined. Except those in loops 1 and 9, all coupons with weight losses exhibited porous near-surface regions. Figure 7 shows such a surface from a coupon at the maximum temperature position (600°C) in a type 316 stainless steel loop. In contrast, no porosity was found in near-surface areas of a coupon from a similar position in a type 304L stainless steel loop [see Fig. 7(b)]. Increased levels of N in the Li did not seem to affect the type of corrosive attack (see Fig. 8), while the addition of Al resulted in surface layers like the one shown in Fig. 9. Electron microprobe analysis revealed that this region was enriched in Ni and Al.

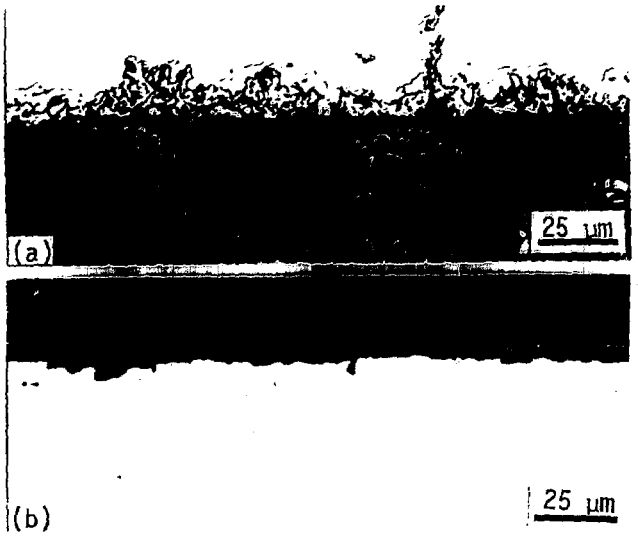

FIGURE 7. Cross Sections of Stainless Steel Insert Coupons Exposed to Flowing Lithium for 3000 h at 600°C. (a) Type 316. (b) Type 304L.

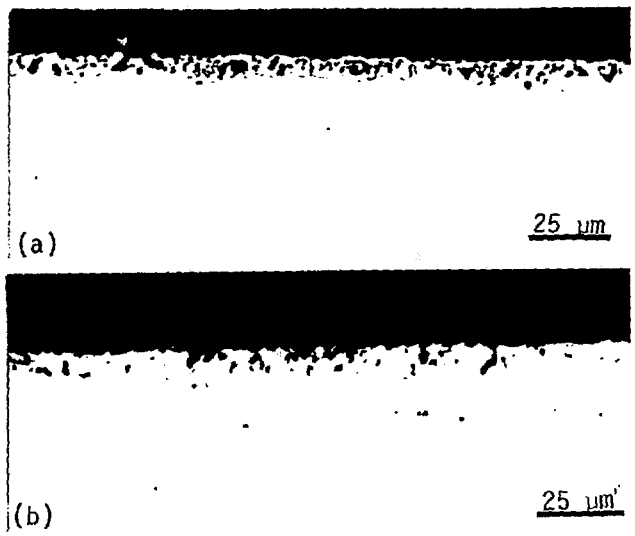

FIGURE 8. Cross Sections of Type 316 Stainless Steel Insert Coupons Exposed for 3000 h to Flowing Nitrogen-Containing Lithium. (a) 1700 wt ppm N, T_{max} = 600°C. (b) 500 wt ppm N, T_{max} = 590°C.

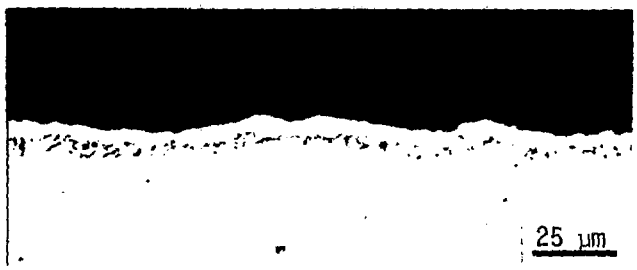

FIGURE 9. Cross Section of a Type 316 Stainless Steel Insert Coupon Exposed to Flowing Li-5 wt % Al for 3000 h at 600°C.

DISCUSSION

In an earlier study[4] of the effect of time on the corrosion rate of type 316 stainless steel in Li thermal-convection loops, the rate decreased during an initial period (1000–2500 h) and then became constant with time. In the present studies, specimens were examined only after 3000 and 10,000 h. Maximum weight losses after these

time periods are compared in Fig. 10 for type 316 stainless steel loops operated at 600°C. Note that, in accordance with the results reported previously, the average rate over the initial 3000-h period, 10.9 mg/m^2 (slope of line A in Fig. 10), is more than twice that over 10,000 h, 4.7 mg/m^2 (slope of line B).

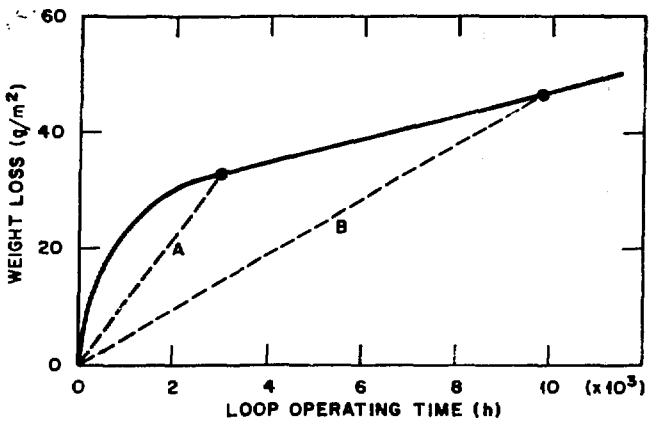

FIGURE 10. Weight Loss vs Loop Operating Time for Type 316 Stainless Steel in Flowing Lithium at 600°C. Slopes of lines A and B give the aveage rates for the two exposure times.

In all tests, specimens from the hotter loop regions were depleted in Ni and Cr and, consequently, enriched in Fe (see Fig. 5, for example). This depletion caused a destabilization of the austenitic phase and led to the formation of ferrite (α-iron). Similar behavior, although to a lesser depth, has been observed[5] for these alloys in Na. Since α-iron is a magnetic phase, we were able to correlate magnetic susceptibility with near-surface ferrite concentration, which appeared to be proportional to weight loss up to 3000 h (see Fig. 6).

Brush[6] has equated the onset of a constant corrosion rate in Na–stainless steel systems to the time when the relative amounts of Ni, Cr, and Fe dissolving in Na

reach the same proportions as the bulk concentrations of the elements in the stainless steel. The ferrite layer increases in thickness until this steady-state condition is reached and remains constant thereafter. We observed that the thickness of the ferrite layer formed on type 316 stainless steel at 600°C did not increase between 3000 and 10,000 h. On this basis we assume that there is no appreciable change in surface concentration after 3000 h and that the ratio of the corrosion rates of Fe, Ni, and Cr has become equal to the ratio of the bulk concentrations in the steel and, therefore, constant with time.

Dissolution rates of types 304L and 316 stainless steel were compared in thermal-convection loops of the respective steels operated under nearly identical conditions (see Table II). Although the maximum corrosion rates differ little between the two steels, it may be significant that the type 316 stainless steel had the lower corrosion rate since this observation would be consistent with the finding by Eremias and Fresl[7] that the corrosion rates of steels in flowing Na increased with decreasing amounts of stabilizing elements (in this case, Mo). Although the weight changes for the two steels were similar, the resulting surface microstructures were different. The ferrite layer on the type 304L stainless steel had very little porosity [Fig. 7(b)] while the layer on the type 316 was extremely porous [Fig. 7(a)]. A porous ferrite layer was also observed on type 321 stainless steel tested under similar conditions,[8] and the development of porosity could be tied to the presence of stabilizing elements (Mo, Ti). A similar observation regarding surface porosity was made in Na systems and led Stoneham[9] to

hypothesize that the stabilizing additives (Mo and Ti) allow the nucleation of cavities in the grain boundaries. Careful metallographic examination of the near-surface region of exposed type 316 stainless steel revealed small cavities at grain boundaries that may have served as the nuclei for the larger voids seen in Fig. 7.

The mass transfer rate of a given element i in a liquid metal system is conventionally described in terms of the rate equation:

$$R_i(x) = k(C_s - C_x) \ , \qquad (1)$$

where

$R_i(x)$ = the dissolution (or deposition) rate (g/m^2h) of element i at point x in the circuit,

k = a temperature-dependent rate constant (m/h) for dissolution (k_s) or deposition (k_p),

C_s = the solubility of element i in Li at temperature T, and

C_x = the concentration of i in Li at point x in the circuit.

For any element, in a closed system where deposition takes place over an area A_p and dissolution over A_s:

$$\int_{A_s} k_s(C_s - C_x)_s \, 2\pi r \, dx - \int_{A_p} k_p(C_s - C_x)_p \, 2\pi r \, dx = G \ , \qquad (2)$$

where

r = the inside tube radius and

G = net increase of element i in the circuit per unit time.

Typically, at steady-state $G \approx 0$, so that

$$\int_{X_1}^{X_2} k_s(C_s - C_x)_s \, dx \approx \int_{X_2}^{X_1} k_p(C_s - C_x)_p \, dx \, . \quad (3)$$

Therefore, the ratio of the average $C_s - C_x$ for dissolution to that for deposition depends on the ratio of the average deposition and dissolution rate constants, k_p/k_s: that is,

$$(C_s - C_x)_s/(C_s - C_x)_p \propto k_p/k_s \, . \quad (4)$$

Given the magnitude of the weight changes in the present tests, C_x does not vary significantly around the circuit relative to the magnitude of $C_s - C_x$; that is, we can neglect the variation of C_x with x. Although C_s increases exponentially with temperature, for this discussion we will regard the dependence as approximately linear within the relatively small temperature interval of our test. Since temperature varies approximately linearly with distance along the loop, C_s will increase or decrease proportionally with distance x from some arbritrary reference point along the loop. For convenience we take our reference points where $C_s = C_x$, which are the points of zero weight change. These balance points divide the area of dissolution from the area of deposition. Note that under the above assumptions, the difference between the maximum loop temperature and the temperature at which zero weight change occurred establishes the magnitude of $(C_s - C_x)_s$; likewise the difference between the minimum loop temperature and the zero weight change temperature establishes

$(\overline{C_s - C_x})_p$. We know, therefore, that the larger the ratio of the dissolution area to deposition area, the larger must be the ratio $(\overline{C_s - C_x})_s/(\overline{C_s - C_x})_p$, and by Eq. (4) the larger the ratio $\bar{k}_p/\bar{k}_s$.

In considering the present mass transfer results in terms of the above rate equations, several general observations are significant;

1. The deposition area increases and the dissolution area decreases between 3000 and 10,000 h.

2. The extent to which surface depletion of Ni occurs in the hot zone is not very sensitive to T_{max}, but the extent of Cr depletion depends very much on this temperature.

3. In all the loop experiments the Cr starts to deposit from the Li at a higher temperature than does Ni.

4. Enhanced N concentrations in the Li may slightly increase the area over which dissolution takes place and correspondingly decrease the deposition area.

As discussed previously, the ferrite layer on type 316 stainless steel inserts from the 600°C loop tests appeared to reach a limiting thickness by 3000 h. We interpreted this observation to imply that the local corrosion rates had reached steady state (became constant with time) within this time period. From Eq. (3) this steady-state assumption would mean that the deposition and dissolution areas should also remain constant with time. The differences in these areas between the 3000- and 10,000-h tests, however, would not be unexpected because of the contribution of transient or non-steady-state behavior to the 3000-h test results.

Table IV indicates that the extent of Cr depletion at a T_{max} of 500°C was

considerably less than that at higher temperatures, while the depletion of Ni was significant even at 500°C. This difference in the temperature dependence of Cr and Ni depletion does not correlate with any radical change in the temperature dependence of Cr and Ni solubilities over this temperature range (see, for example, ref. 10). Therefore, since the steady-state ratio of Ni and Cr fluxes must be constant with temperature (see above), this difference must be due either to a difference in the relative response of the dissolution rate constants to temperature or to differences in deposition kinetics which affect C_x relative to C_s [see Eq. (1)]. The latter possibility can be assessed by considering the effect of loop temperature on the locations of the points at which the Cr surface concentration equals the bulk concentration (balance points), as shown in Table IV. Note the increase in the relative areas of Cr dissolution compared with deposition as T_{max} increases from 600 to 650°C. As discussed above, the increase in the ratio of dissolution to deposition area for Cr implies a change in the relative magnitudes of the respective rate constants, k, in Eq. (4) such that $\bar{k}_p$ increases relative to $\bar{k}_s$ as the temperature is increased. This implies that $\bar{k}_p$ increases with temperature more than does $\bar{k}_s$, since a decrease in either rate constant with increasing temperature is inconsistent with the expected temperature response of the physical processes controlling mass transfer in these systems. The insensitivity of Ni depletion to maximum loop temperature implies that both the dissolution and deposition processes change in approximately the same

proportion as a function of temperature and both play a role in the transfer of Ni around the circuit.

The data in Table IV also show that the deposition area for Cr was larger than that for Ni in every loop. According to Eq. (4), this observation implies that

$$(\bar{k}_p/\bar{k}_s)_{Cr} < (\bar{k}_p/\bar{k}_s)_{Ni} . \qquad (5)$$

This relationship is consistent with the above-mentioned behavior in which deposition appears to be relatively more sluggish (that is, rate-controlling) than dissolution for Cr transfer around a loop, while the dissolution and deposition processes appear more equally balanced in determining Ni transfer.

The depletion in Ni and Cr at surfaces undergoing dissolution is accompanied by an enrichment of Fe at the surface relative to its bulk concentration in the stainless steel (Table IV). This observation coupled with a dissolution rate that is independent of time implies that the rate of Fe dissolution is controlled either by a chemical reaction at the surface of by Fe diffusion in the Li, and not by solid-state diffusion. Further support for this conclusion is given by the activation energy derived for the four type 316 stainless steel thermal-convection loops operated for 300°h. Solid-state diffusion processes characteristically require an activation energy in the range from 170 to 320 kj/mol. However, our results yielded an apparent activation energy of 60 kj/mol, which may be consistent with diffusion of Fe through the liquid Li boundary layer.[4]

Two loop tests in this series were operated with relatively large initial N concentrations in the Li (Table III). In both cases the surface areas for dissolution

were greater and the maximum corrosion rates were smaller than in tests with purer Li at the same temperature. Although the limited amount of available data[10] indicates that the solubilities of Cr and Ni in Li increase with increasing N concentration of the Li, no consistent trend has been established[10] for the solubility of Fe and Li. It is therefore difficult to interpret these results in terms of Eq. (4); nevertheless, the presence of N in Li conceivably acts to decrease the magnitude of k_s for the overall system. It is important to note that the effects of N additions to Li in these loop tests were very different from the effects of N in Li observed in static capsule tests.[11] In these tests N additions caused general dissolution of type 316 stainless steel at 500°C and grain boundary attack at 600 and 700°C. However, those effects were produced only at initial N concentrations generally above those reached in the loop tests and occurred at surfaces that were not severely depleted of Cr and Ni.

The effect of Al in Li on the corrosion rate in these loop tests was dramatic: the mass transfer rate of type 316 stainless steel at 600°C decreased by a factor greater than 5 (see Table III). The Al reacted rapidly with the stainless steel in the hotter loop regions to form a thin surface layer (see Fig. 9). Electron microprobe analysis revealed that the Al reacted primarily with the Ni and to a lesser extent with the Fe. The details of this surface layer and its effect on corrosion rates are given elsewhere.[12,13] It does appear to be an effective and easily implemented method of reducing mass transfer in Ni-bearing alloy-Li systems and possibly for other Fe-base structural alloys.

One important test parameter that could not be treated in these loop tests was the Li velocity. The present results are relevant to Li systems such as semistagnant tritium-breeding blankets for fusion applications. However, to the extent that Fe dissolution rates are controlled by diffusion in the Li, significantly greater corrosion rates can be expected in faster flowing Li systems.

SUMMARY

Lithium in stainless steel thermal-convection loops with insert specimens in the heated and cooled regions were used to study the kinetics of mass transfer by analysis of weight changes and surface compositions. Both Ni and Cr were preferentially leached from the stainless steel in the hot zone; however, Cr transfer depended much more on loop operating temperature than Ni transfer. The ratio of the average deposition rate constant to the average dissolution rate constant for Cr was less than this ratio for Ni.

The leaching of Ni and Cr resulted in a ferrite layer at the exposed surfaces of specimens in the hotter loop sections. The thickness of this layer apeared to attain a steady state within 3000 h. This implies that the net flux of Ni, Cr, and Fe moving into and out of this layer remains constant with time and that, therefore, the composition at any point below the surface must be fixed with time. The latter condition requires that the corrosion process be stoichiometric; that is, Fe, Cr, and Ni dissolve in the same proportional as their respective concentrations in the stainless steel. The activation energy for the overall mass transfer process in these loops was about 60 kJ/mol. This energy is

consistent with a dissolution and/or deposition process where the rate of movement of Fe is controlled by liquid-phase diffusion.

The main effect of enhanced N concentration in Li was to increase the area over which dissolution took place and therby decrease the magnitude of the mass transfer rate constant for dissolution. Porosity in the near-surface ferrite layer at 600°C was relativley dense for type 316 stainless steel and nearly absent for type 304L stainless steel. The porosity may be associated with the presence of carbide-forming metals other than Cr. The addition of 5 wt % Al to Li resulted in a fivefold decrease in the mass transfer rate of type 316 stainless steel in Li flowing between 400 and 600°C.

ACKNOWLEDGMENTS

The authors acknowledge the experimental work of H. D. Upton and the metallographic assistance of M. D. Allen and J. R. Mayotte. They wish to thank J. R. DiStefano and M. L. Grossbeck for their reviews of the manuscript, S. Peterson for the editing, and P. J. Dickens for report preparation.

REFERENCES

1. M. S. Freed and K. J. Kelly (eds.), *Corrosion of Columbian Base and Other Structural Alloys in High Temperature Lithium,* PWAC-355, Pratt and Whitney, June 1961.

2. J. H. DeVan, J. E. Selle, and A. E. Morris, *Review of Lithium Iron-Base Alloy Corrosion Studies,* ORNL/TM-4927, Oak Ridge National Laboratory, January 1976.

3. P. F. Tortorelli, J. H. DeVan, and J. E. Selle, *Corrosion of Austenitic Stainless Steels in Flowing Lithium,* (report in preparation).

4. P. F. Tortorelli and J. H. DeVan, "Thermal-Gradient Mass Transfer in Lithium-Stainless Steel Systems," *J. Nucl. Mater.* 85 and 86, 189–93, 1979.

5. J. R. Weeks and H. S. Isaacs, "Corrosion and Deposition of Steels and Nickel-Base Alloys in Liquid Sodium," pp. 1–66 in *Advances in Corrosion Science and Technology*, Vol. 3, 1973.

6. E. G. Brush, *Sodium Mass Transfer XVI. The Selective Corrosion Component of Steel Exposed to Flowing Sodium,* GEAP-4832, General Electric, March 1965.

7. B. Eremias and M. Fresl, "Influence of the Chemical Composition of Austenitic Stainless Steel on Their Corrosion Behaviour in High Temperature Sodium," *J. Nucl. Mater.* 75, 186–92 (1978).

8. J. E. Selle, "Corrosion of Iron-Base Alloys by Lithium," pp. 453–61 in *Proc. Int. Conf. Liquid Metal Technol. Energy Production,* CONF-760503-P2 (May 1976).

9. A. M. Stoneham, *Formation of Cavities in Steels Exposed to Liquid Sodium,* AERE-R-7734, Atomic Energy Research Establishment, May 1974.

10. D. F. Anthrop, *The Solubilities of Transition Metals in Liquid Alkali and Alkaline Earth Metals, Lanthanum and Cerium / Critical Review of the Literature,* UCRL-50315, Lawrence Livermore Laboratory, September 1967.

11. P. F. Tortorelli, J. H. DeVan, and J. E. Selle, "Effects of Nitrogen and Nitrogen Getters in Lithium on the Corrosion of Type 316 Stainless Steel," paper 115, *NACE Corrosion/79* (Atlanta, Georgia, March 12–16, 1979).

12. P. F. Tortorelli and J. H. DeVan, *ADIP Quarterly Progress Report*, DOE/ET-0058/7, Department of Energy, September 1979, pp. 170–74.

13. P. F. Tortorelli, J. H. DeVan, J. E. Selle, and H. D. Upton, "Corrosion Inhibition in Systems of Lithium with Ni-Bearing Alloys," to be published in the preceedings of the *8th Symposium Engineering Problems of Fusion Research*, Held by IEEE, 12–16, 1979, San Francisco, Calif.